



ELSEVIER

Available online at www.sciencedirect.com

SCIENCE @ DIRECT®

Journal of Sound and Vibration 291 (2006) 539–565

JOURNAL OF
SOUND AND
VIBRATION

www.elsevier.com/locate/jsvi

Theory and experiments for large-amplitude vibrations of rectangular plates with geometric imperfections

M. Amabili*

Dipartimento di Ingegneria Industriale, Università di Parma, Parco Area delle Scienze 181/A, Parma, 43100 Italy

Received 30 March 2005; received in revised form 16 June 2005; accepted 16 June 2005

Available online 6 September 2005

Abstract

Large-amplitude vibrations of rectangular plates subjected to harmonic excitation are investigated. The von Kármán nonlinear strain–displacement relationships are used to describe the geometric nonlinearity. A specific boundary condition, with restrained normal displacement at the plate edges and fully free in-plane displacements, not previously considered, has been introduced as a consequence that it is very close to the experimental boundary condition. Results for this boundary condition are compared to nonlinear results previously obtained for: (i) simply supported plates with immovable edges; (ii) simply supported plates with movable edges, and (iii) fully clamped plates. The nonlinear equations of motion are studied by using a code based on pseudo-arclength continuation method. A thin rectangular stainless-steel plate has been inserted in a metal frame; this constraint is approximated with good accuracy by the newly introduced boundary condition. The plate inserted into the frame has been measured with a 3D laser system in order to reconstruct the actual geometry and identify geometric imperfections (out-of-planarity). The plate has been experimentally tested in laboratory for both the first and second vibration modes for several excitation magnitudes in order to characterize the nonlinearity of the plate with imperfections. Numerical results are able to follow experimental results with good accuracy for both vibration modes and for different excitation levels once the geometric imperfection is introduced in the model. Effects of geometric imperfections on the trend of nonlinearity and on natural frequencies are shown; convergence of the solution with the number of generalized coordinates is numerically verified.

© 2005 Elsevier Ltd. All rights reserved.

*Tel.: +39 0521 905 896; fax: +39 0521 905 705.

E-mail address: marco@me.unipr.it.

URL: <http://me.unipr.it/mam/amabili/amabili.html>.

1. Introduction

Extensive literature reviews on the nonlinear vibration of plates are given by Chia [1], Sathyamoorthy [2] and Chia [3]; curved panels and shells are reviewed by Amabili and Païdoussis [4]. The fundamental study in the analysis of large-amplitude vibrations of rectangular plates is due to Chu and Hermann [5], who were the pioneers in the field. They studied the fundamental mode of simply supported rectangular plates with immovable edges with different aspect ratios. The solution was obtained by using a perturbation analysis and shows strong hardening-type nonlinearity.

A series of interesting papers [6–9] compared the backbone curves of the fundamental mode of isotropic plates with the results of Chu and Hermann [5]; all of them are in good agreement with the original results of Chu and Hermann. In particular, Leung and Mao [8] also studied simply supported rectangular plates with movable edges, which present reduced hardening-type nonlinearity with respect to simply supported plates with immovable edges.

The effect of geometric imperfection was investigated by Hui [10]. Yasuda and Asano [11] studied rectangular membranes with internal resonances (one-to-one) both numerically and experimentally. One-to-one internal resonances and chaos in harmonically excited rectangular plates were studied numerically by Chang et al. [12].

Recent studies by Han and Petyt [13,14] and Ribeiro and Petyt [15–17] used the hierarchical finite element method to deeply investigate the nonlinear response of clamped rectangular plates. A similar approach was used by Ribeiro [18] to investigate the forced response of simply supported plates with immovable edges. A simplified analytical approach was developed by El Kadiri and Benamar [19] for the case previously studied by Chu and Hermann.

Recently, Amabili [20] compared results for nonlinear forced vibrations of rectangular plates with the following boundary conditions: (i) simply supported plates with movable edges; (ii) simply supported plates with immovable edges, and (iii) fully clamped plates. Results show that in all the three cases the response is of hardening-type. However, in case (i) there is a mild nonlinearity, which becomes strong in case (ii) and extremely strong in case (iii) for the clamped plate. Experimental responses for the fundamental mode of an aluminum rectangular plate obtained for different excitations are provided and compared with reasonable agreement to numerical simulations. The effect of geometric imperfections, taken into account in the theory, was not investigated in both the experimental and numerical results. Even if a large number of theoretical studies on large-amplitude vibrations of rectangular plates are available in the scientific literature, experimental results are very scarce and those reported by Amabili [20] seem to be the most suitable to reconstruct the trend of nonlinearity.

As a consequence of this lack in the literature, a new series of experiments has been designed by using more sophisticated instrumentation and measurement of the actual surface geometry of the experimental plate has been carried out. The present paper synthesizes the experimental results, the theory developed and the numerical simulations. A specific boundary condition, with restrained normal displacement at the plate edges and fully free in-plane displacements, not previously considered in Ref. [20], has been introduced as a consequence that it is very close to the experimental boundary condition. Results for this boundary condition are compared to nonlinear results previously obtained in Ref. [20] for different boundary conditions. The plate inserted into the frame has been measured with a 3D laser system in order to reconstruct the actual geometry

and identify geometric imperfections (out-of-planarity). The plate has been experimentally tested in laboratory for both the first and second vibration modes for several excitation magnitudes in order to characterize the nonlinearity of the plate with imperfections. Numerical results are able to predict experimental results with good accuracy for both vibration modes and for different excitation levels once the geometric imperfection is introduced in the model. Effects of geometric imperfections on the trend of nonlinearity and on natural frequencies are shown; convergence of the solution with the number of generalized coordinates is numerically verified.

2. Elastic strain energy of the plate

A rectangular plate with coordinate system (O; x , y , z), having the origin O at one corner is considered. The displacements of an arbitrary point of coordinates (x , y) on the middle surface of the plate are denoted by u , v and w , in the x , y and normal (z) directions, respectively. Initial geometric imperfections of the rectangular plate associated with zero initial tension are denoted by normal displacement w_0 ; in-plane initial imperfections are neglected.

The von Kármán nonlinear strain–displacement relationships are used. The strain components ε_x , ε_y and γ_{xy} at an arbitrary point of the plate are related to the middle surface strains $\varepsilon_{x,0}$, $\varepsilon_{y,0}$ and $\gamma_{xy,0}$ and to the changes in the curvature and torsion of the middle surface k_x , k_y and k_{xy} by the following three relationships

$$\varepsilon_x = \varepsilon_{x,0} + zk_x, \quad \varepsilon_y = \varepsilon_{y,0} + zk_y, \quad \gamma_{xy} = \gamma_{xy,0} + zk_{xy}, \quad (1)$$

where z is the distance of the arbitrary point of the plate from the middle surface. According to von Kármán's theory, the middle surface strain–displacement relationships and changes in the curvature and torsion are given by [21]

$$\varepsilon_{x,0} = \frac{\partial u}{\partial x} + \frac{1}{2} \left(\frac{\partial w}{\partial x} \right)^2 + \frac{\partial w}{\partial x} \frac{\partial w_0}{\partial x}, \quad (2a)$$

$$\varepsilon_{y,0} = \frac{\partial v}{\partial y} + \frac{1}{2} \left(\frac{\partial w}{\partial y} \right)^2 + \frac{\partial w}{\partial y} \frac{\partial w_0}{\partial y}, \quad (2b)$$

$$\gamma_{xy,0} = \frac{\partial u}{\partial y} + \frac{\partial v}{\partial x} + \frac{\partial w}{\partial x} \frac{\partial w}{\partial y} + \frac{\partial w}{\partial x} \frac{\partial w_0}{\partial y} + \frac{\partial w_0}{\partial x} \frac{\partial w}{\partial y}, \quad (2c)$$

$$k_x = -\frac{\partial^2 w}{\partial x^2}, \quad (2d)$$

$$k_y = -\frac{\partial^2 w}{\partial y^2}, \quad (2e)$$

$$k_{xy} = -2 \frac{\partial^2 w}{\partial x \partial y}. \quad (2f)$$

The elastic strain energy U_P of a plate, neglecting σ_z under Kirchhoff's hypotheses, is given by

$$U_P = \frac{1}{2} \int_0^a \int_0^b \int_{-h/2}^{h/2} (\sigma_x \varepsilon_x + \sigma_y \varepsilon_y + \tau_{xy} \gamma_{xy}) dx dy dz, \quad (3)$$

where h is the plate thickness, a and b are the in-plane dimensions in x and y directions, respectively, and the stresses σ_x , σ_y and τ_{xy} are related to the strain for homogeneous and isotropic material ($\sigma_z = 0$, case of plane stress) by

$$\sigma_x = \frac{E}{1-\nu^2} (\varepsilon_x + \nu \varepsilon_y), \quad \sigma_y = \frac{E}{1-\nu^2} (\varepsilon_y + \nu \varepsilon_x), \quad \tau_{xy} = \frac{E}{2(1+\nu)} \gamma_{xy}, \quad (4)$$

where E is the Young's modulus and ν is the Poisson's ratio. By using Eqs. (1), (3), and (4), the following expression is obtained

$$U_P = \frac{1}{2} \frac{Eh}{1-\nu^2} \int_0^a \int_0^b \left(\varepsilon_{x,0}^2 + \varepsilon_{y,0}^2 + 2\nu \varepsilon_{x,0} \varepsilon_{y,0} + \frac{1-\nu}{2} \gamma_{xy,0}^2 \right) dx dy + \frac{1}{2} \frac{Eh^3}{12(1-\nu^2)} \int_0^a \int_0^b \left(k_x^2 + k_y^2 + 2\nu k_x k_y + \frac{1-\nu}{2} k_{xy}^2 \right) dx dy + O(h^4), \quad (5)$$

where $O(h^4)$ is a higher-order term in h ; the first term is the membrane (also referred to as stretching) energy and the second one is the bending energy.

3. Boundary conditions, kinetic energy, external loads and mode expansion

The kinetic energy T_P of a rectangular plate, by neglecting rotary inertia, is given by

$$T_P = \frac{1}{2} \rho_P h \int_0^a \int_0^b (\dot{u}^2 + \dot{v}^2 + \dot{w}^2) dx dy, \quad (6)$$

where ρ_P is the mass density of the plate. In Eq. (6) the overdot denotes a time derivative.

The virtual work W done by the external forces is written as

$$W = \int_0^a \int_0^b (q_x u + q_y v + q_z w) dx dy, \quad (7)$$

where q_x , q_y and q_z are the distributed forces per unit area acting in x , y and z directions, respectively. In the present study, only a single harmonic force orthogonal to the plate is considered; therefore $q_x = q_y = 0$. The external distributed load q_z applied to the plate, due to the concentrated force \tilde{f} , is given by

$$q_z = \tilde{f} \delta(y - \tilde{y}) \delta(x - \tilde{x}) \cos(\omega t). \quad (8)$$

where ω is the excitation frequency, t is the time, δ is the Dirac delta function, \tilde{f} is the force magnitude positive in z direction; \tilde{x} and \tilde{y} give the position of the point of application of the force. In the present study, the excitation point is located at $\tilde{x} = a/4$, $\tilde{y} = b/4$, in order to reproduce experiments. Eq. (7) can be rewritten in the following form

$$W = \tilde{f} \cos(\omega t) (w)_{x=a/4, y=b/4}. \quad (9)$$

The following boundary condition is introduced in the present study:

$$N_x = N_{x,y} = w = w_0 = M_x = \partial^2 w_0 / \partial x^2 = 0 \quad \text{at } x = 0, a, \tag{10a-f}$$

$$N_y = N_{x,y} = w = w_0 = M_y = \partial^2 w_0 / \partial y^2 = 0 \quad \text{at } y = 0, b, \tag{11a-f}$$

where M is the bending moment per unit length, N_x and N_y are the normal forces per unit length on the edges orthogonal to x and y , respectively, and $N_{x,y}$ is the shear force per unit length. Eqs. (10) and (11) give fully free in-plane conditions and w is restrained at the plate edges.

In order to reduce the system to finite dimensions, the middle surface displacements u , v and w are expanded by using the following approximate functions, which satisfy identically the geometric boundary conditions (10c) and (11c):

$$w(x, y, t) = \sum_{m=1}^{M_1} \sum_{n=1}^{N_1} w_{m,n}(t) \sin(m\pi x/a) \sin(n\pi y/b), \tag{12}$$

$$u(x, y, t) = \sum_{m=1}^{M_2} \sum_{n=1}^{N_2} u_{m,n}(t) \cos(m\pi x/a) \cos(n\pi y/b), \tag{13}$$

$$v(x, y, t) = \sum_{m=1}^{M_3} \sum_{n=1}^{N_3} v_{m,n}(t) \cos(m\pi x/a) \cos(n\pi y/b), \tag{14}$$

where m and n are the numbers of half-waves in x and y directions, respectively, and t is the time; $u_{m,n}(t)$, $v_{m,n}(t)$ and $w_{m,n}(t)$ are the generalized coordinates that are unknown functions of t . M and N indicate the terms necessary in the expansion of the displacements; in general, more in-plane terms than generalized coordinates $w_{m,n}(t)$ are necessary to describe correctly the trend of nonlinearity [20].

Initial geometric imperfections of the rectangular plate are considered only in z direction. They are associated with zero initial stress. The imperfection w_0 is expanded in the same form of w , i.e. in a double Fourier sine series satisfying the boundary conditions (10d,f) and (11d,f) at the plate edges

$$w_0(x, y) = \sum_{m=1}^{\tilde{M}} \sum_{n=1}^{\tilde{N}} A_{m,n} \sin(m\pi x/a) \sin(n\pi y/b), \tag{15}$$

where $A_{m,n}$ are the modal amplitudes of imperfections; \tilde{N} and \tilde{M} are integers indicating the number of terms in the expansion.

4. Additional terms to satisfy the boundary conditions

The geometric boundary conditions, Eqs. (10c,d,f) and (11c,d,f) are exactly satisfied by the expansions of u , v , w and w_0 . On the other hand, Eqs. (10e) and (11e) can be rewritten in the

following form [21]:

$$M_x = \frac{Eh^3}{12(1 - \nu^2)} (k_x + \nu k_y) = 0 \quad \text{at } x = 0, a, \tag{16}$$

$$M_y = \frac{Eh^3}{12(1 - \nu^2)} (k_y + \nu k_x) = 0 \quad \text{at } y = 0, b, \tag{17}$$

Eqs. (16) and (17) are identically satisfied for the expressions of k_x and k_y given in Eqs. (2d,e). Moreover, the following constraints must be satisfied [21]:

$$N_x = \frac{Eh}{1 - \nu^2} (\varepsilon_{x,0} + \nu \varepsilon_{y,0}) = 0 \quad \text{at } x = 0, a, \tag{18}$$

$$N_y = \frac{Eh}{1 - \nu^2} (\varepsilon_{y,0} + \nu \varepsilon_{x,0}) = 0 \quad \text{at } y = 0, b. \tag{19}$$

Eqs. (18) and (19) are not identically satisfied. Eliminating null terms at the plate edges, Eqs. (18) and (19) can be rewritten as

$$\left[\frac{\partial \hat{u}}{\partial x} + \frac{1}{2} \left(\frac{\partial w}{\partial x} \right)^2 + \frac{\partial w}{\partial x} \frac{\partial w_0}{\partial x} + \nu \frac{\partial \hat{v}}{\partial y} \right]_{x=0,a} = 0, \tag{20}$$

$$\left[\frac{\partial \hat{v}}{\partial y} + \frac{1}{2} \left(\frac{\partial w}{\partial y} \right)^2 + \frac{\partial w}{\partial y} \frac{\partial w_0}{\partial y} + \nu \frac{\partial \hat{u}}{\partial x} \right]_{y=0,b} = 0, \tag{21}$$

where \hat{u} and \hat{v} are terms added to the expansion of u and v , given in Eqs. (13) and (14), in order to satisfy exactly the boundary conditions $N_x = 0$ and $N_y = 0$. As a consequence that \hat{u} and \hat{v} are second-order terms in the plate displacement, they have not been inserted in the second-order terms that involve u and v in Eqs. (20) and (21). Non-trivial calculations, reported in Ref. [22] for a different geometry, give

$$\begin{aligned} \hat{u}(t) = & - \sum_{n=1}^{N_1} \sum_{m=1}^{M_1} (m\pi/a) \left\{ \frac{1}{2} w_{m,n}(t) \sin(n\pi y/b) \sum_{k=1}^{N_1} \sum_{s=1}^{M_1} \frac{s}{m+s} w_{s,k}(t) \sin(k\pi y/b) \sin[(m+s)\pi x/a] \right. \\ & \left. + w_{m,n}(t) \sin(n\pi y/b) \sum_{j=1}^{\tilde{N}} \sum_{i=1}^{\tilde{M}} \frac{i}{m+i} A_{i,j} \sin(j\pi y/b) \sin[(m+i)\pi x/a] \right\}, \tag{22} \end{aligned}$$

$$\begin{aligned} \hat{v}(t) = & - \sum_{n=1}^{N_1} \sum_{m=1}^{M_1} (n\pi/b) \left\{ \frac{1}{2} w_{m,n}(t) \sin(m\pi x/a) \sum_{k=1}^{N_1} \sum_{s=1}^{M_1} \frac{k}{n+k} w_{s,k}(t) \sin(s\pi x/a) \sin[(n+k)\pi y/b] \right. \\ & \left. + w_{m,n}(t) \sin(m\pi x/a) \sum_{j=1}^{\tilde{N}} \sum_{i=1}^{\tilde{M}} \frac{j}{n+j} A_{i,j} \sin(i\pi x/a) \sin[(n+j)\pi y/b] \right\}. \tag{23} \end{aligned}$$

Finally boundary conditions (10b) and (11b) must be also satisfied. They give [21]

$$N_{x,y} = N_{y,x} = \frac{Eh}{2(1 + \nu)} \gamma_{x,y} = 0, \quad \text{at } x = 0, a, \text{ and at } y = 0, b. \tag{24}$$

Eliminating null terms at the plate edges, Eq. (24) can be rewritten as

$$\left[\frac{\partial u}{\partial y} + \frac{\partial v}{\partial x} \right]_{\substack{x=0,a \\ \text{or} \\ y=0,b}} = 0. \tag{25}$$

Eq. (25) is a linear condition, which is satisfied by using minimization of energy in the Lagrange equations of motion. Therefore no additional terms in the expansion are introduced. Actually, also Eqs. (18) and (19) can be satisfied by energy minimization by avoiding to introduce Eqs. (22) and (23). But in this case the choice of the expansions of u and v become very tricky, i.e. all the terms involved in Eqs. (22) and (23) must be inserted in the expansion in order to predict the system behavior with accuracy. This has been verified numerically.

5. Lagrange equations of motion

The non-conservative damping forces are assumed to be of viscous type and are taken into account by using the Rayleigh’s dissipation function

$$F = \frac{1}{2} c \int_0^a \int_0^b (\dot{u}^2 + \dot{v}^2 + \dot{w}^2) dx dy, \tag{26}$$

where c has a different value for each term of the mode expansion. Simple calculations give

$$F = \frac{1}{2} (ab/4) \left[\sum_{n=1}^{N_1} \sum_{m=1}^{M_1} c_{m,n} \dot{w}_{m,n}^2 + \sum_{n=1}^{N_2} \sum_{m=1}^{M_2} c_{m,n} \dot{u}_{m,n}^2 + \sum_{n=1}^{N_3} \sum_{m=1}^{M_3} c_{m,n} \dot{v}_{m,n}^2 \right]. \tag{27}$$

The damping coefficient $c_{m,n}$ is related to modal damping ratio (in this case it is a damping ratio of the generalized coordinate), that can be evaluated from experiments, by $\zeta_{m,n} = c_{m,n}/(2\mu_{m,n}\omega_{m,n})$, where $\omega_{m,n}$ is the natural circular frequency of mode (m, n) and $\mu_{m,n}$ is the mass associated with this generalized coordinate, given by $\mu_{m,n} = \rho_S h(ab/4)$.

The following notation is introduced for brevity:

$$\mathbf{q} = \{u_{m,n}, v_{m,n}, w_{m,n}\}^T, \quad m = 1, \dots, M_{1 \text{ or } 2 \text{ or } 3} \text{ and } n = 1, \dots, N_{1 \text{ or } 2 \text{ or } 3}. \tag{28}$$

The generic element of the time-dependent vector \mathbf{q} is referred to as q_j , which is the generalized coordinate; the dimension of \mathbf{q} is dofs, which is the number of degrees of freedom used in the mode expansion.

The generalized forces Q_j are obtained by differentiation of the Rayleigh’s dissipation function and of the virtual work done by external forces

$$Q_j = -\frac{\partial F}{\partial \dot{q}_j} + \frac{\partial W}{\partial q_j} = -(ab/4)c_j \dot{q}_j + \begin{cases} 0 & \text{if } q_j = u_{m,n}, v_{m,n}; \text{ or } w_{m,n} \text{ with } m \text{ or } n = 4, 8, \dots, \\ \alpha \tilde{f} \cos(\omega t) & \text{if } q_j = w_{m,n} \text{ with } m \text{ or } n \neq 4, 8, \dots, \end{cases} \tag{29}$$

where α is a coefficient taking the opportune numerical value ($\pm 1, \pm\sqrt{2}/2, \pm 1/2$) according with the value of (m, n) . The Lagrange equations of motion are

$$\frac{d}{dt} \left(\frac{\partial T_P}{\partial \dot{q}_j} \right) - \frac{\partial T_P}{\partial q_j} + \frac{\partial U_P}{\partial q_j} = Q_j, \quad j = 1, \dots, \text{dofs}, \quad (30)$$

where $\partial T_P / \partial q_j = 0$. These second-order equations have very long expressions containing quadratic and cubic nonlinear terms. In particular,

$$\frac{d}{dt} \left(\frac{\partial T_P}{\partial \dot{q}_j} \right) = \rho_P h (ab/4) \ddot{q}_j, \quad (31)$$

which shows that no inertial coupling among the Lagrange equations exists for the plate with the mode expansion used.

The very complicated term giving quadratic and cubic nonlinearities can be written in the form

$$\frac{\partial U}{\partial q_j} = \sum_{k=1}^{\text{dofs}} q_k f_k + \sum_{i,k=1}^{\text{dofs}} q_i q_k f_{i,k} + \sum_{i,k,l=1}^{\text{dofs}} q_i q_k q_l f_{i,k,l}, \quad (32)$$

where coefficients f have long expressions that include also geometric imperfections. Quadratic nonlinearities of the type q_i^2 (in particular for $q_i = w_{m,n}$) are never present in the equations of motion of perfect flat plates. This is a difference with respect to curved panels [22] and it is physically explained by the fact that no different displacement is observed for flat plates in z and $-z$ directions, due to the symmetry. Presence of quadratic nonlinearities is the reason for significant asymmetric displacement in z and $-z$ that is observed in the results of this study presented in the following sections. Numerical results show that, for very thin plates, geometric imperfections of the magnitude of the plate thickness give quadratic terms with an effect of the same order of cubic terms, for vibration amplitude of the order of the plate thickness. Therefore the classical hardening-type nonlinearity, which is characteristics of flat plates, is transformed by significant imperfections into softening-type nonlinearity, turning to hardening-type for larger vibration amplitudes.

The equations of motion have been obtained by using the *Mathematica* version 4 computer software [23] in order to perform analytical surface integrals of trigonometric functions (e.g. integrals in Eq. (5)). The generic j th Lagrange equation is divided by the modal mass associated with \ddot{q}_j and then is transformed in two first-order equations. A non-dimensionalization of variables is also performed for computational convenience: the frequencies are divided by the natural radian frequency $\omega_{m,n}$ of the mode (m, n) investigated, and the vibration amplitudes are divided by the plate thickness h . The resulting $2 \times \text{dofs}$ equations are studied by using (i) the software AUTO 97 [24] for continuation and bifurcation analysis of nonlinear ordinary differential equations, and (ii) direct integration of the equations of motion by using the DIVPAG routine of the Fortran library IMSL. The software AUTO 97 is capable of continuation of the solution, bifurcation analysis and branch switching by using pseudo-arclength continuation and collocation methods. In particular, the plate response under harmonic excitation has been studied by using an analysis in two steps: (i) first the excitation frequency has been fixed far enough from resonance and the magnitude of the excitation has been used as bifurcation parameter; the

solution has been started at zero force where the solution is the trivial undisturbed configuration of the plate and has been continued up to reach the desired force magnitude; (ii) when the desired magnitude of excitation has been reached, the solution has been continued by using the excitation frequency as bifurcation parameter.

6. Numerical results: effect of boundary conditions on the trend of nonlinearity for perfect plate

Calculations have been initially performed for a rectangular aluminum plate without imperfections with the following dimensions and material properties: $a = 0.515$ m, $b = 0.184$ m, $h = 0.0003$ m, $E = 69 \times 10^9$ Pa, $\rho = 2700$ kg/m³ and $\nu = 0.33$. This plate has fundamental mode ($n = 1, m = 1$) with radian frequency $\omega_{1,1} = 24.26 \times 2\pi$ rad/s and it has been previously studied in Ref. [20] for the following three boundary conditions: (i) simply supported with movable edges; (ii) simply supported with immovable edges; and (iii) fully clamped. In the present study, the new boundary conditions introduced in Eqs. (10) and (11), i.e. fully free in-plane displacement, is considered for harmonic excitation around the fundamental resonance, at the plate center (at $x = a/2$ and $y = b/2$), of magnitude $\tilde{f} = 0.007$ N, assuming modal damping $\zeta_{1,1} = 0.0117$ (the same damping ratio is assumed for all the generalized coordinates). The maximum plate oscillation at the center of the plate (almost coincident with $w_{1,1}$ in this case) is presented in Fig. 1 and is compared to results obtained in Ref. [20] for the other three boundary conditions. It is evident that the new boundary condition gives mild hardening-type nonlinearity, even reduced

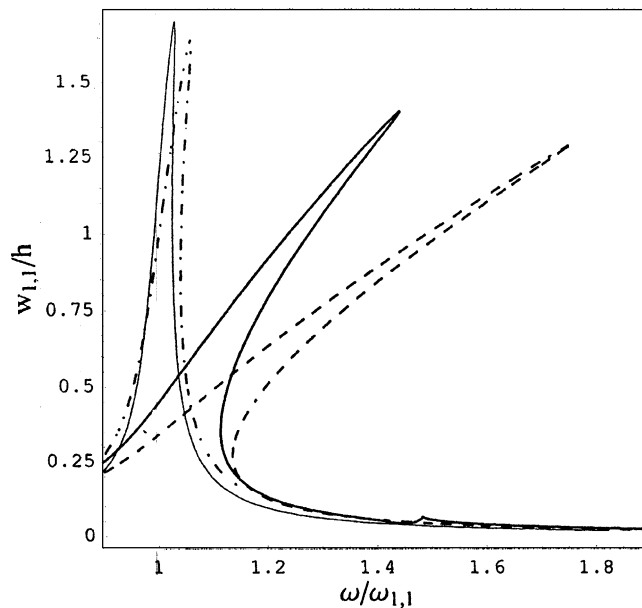


Fig. 1. Response of the plate with different boundary conditions; mode (1, 1). —, present study, plate with fully free in-plane displacement, $\tilde{f} = 0.007$ N, $\zeta_{1,1} = 0.0117$, 22 dofs; - - -, simply supported plate with movable edges, $\tilde{f} = 0.007$ N, $\zeta_{1,1} = 0.0117$, 12 dofs, [20]; - · -, simply supported plate with immovable edges, $\tilde{f} = 0.007$ N, $\zeta_{1,1} = 0.0147$, 16 dofs, [20]; —, clamped plate, $\tilde{f} = 0.0467$ N, $\zeta_{1,1} = 0.0147$, 39 dofs, [20].

with respect to the one of the simply supported plate with movable edges. In fact, the reduced in-plane constraint decreases the nonlinearity of the plate. Present results have been obtained by using a model with 22 dof, i.e. with 22 generalized coordinates. In particular, they are: $w_{1,1}$, $w_{1,3}$, $w_{3,1}$, $w_{3,3}$, $u_{1,0}$, $u_{1,2}$, $u_{1,4}$, $u_{3,0}$, $u_{3,2}$, $u_{3,4}$, $u_{5,0}$, $u_{5,2}$, $u_{5,4}$, $v_{0,1}$, $v_{2,1}$, $v_{4,1}$, $v_{0,3}$, $v_{2,3}$, $v_{4,3}$, $v_{0,5}$, $v_{2,5}$, $v_{4,5}$.

7. Experimental set-up and results

Tests have been conducted on an almost squared, stainless steel plate with the following dimensions and material properties: $a = 0.2085$ m, $b = 0.21$ m, $h = 0.0003$ m, $E = 198 \times 10^9$ Pa, $\rho = 7850$ kg/m³ and $\nu = 0.3$. The plate was inserted into a heavy rectangular steel frame made of several thick parts, see Fig. 2, having grooves designed with V shape to hold the plate and avoid out-of-plane displacements at the edges. Silicon was placed into the grooves to better fill any possible gap between the grooves and the plate. Practically all the in-plane displacements at the edges were allowed because the constraint given by silicon on in-plane displacements is small. Therefore the experimental boundary conditions are close to those given by Eqs. (10) and (11).

The plate has been subjected to (i) burst-random excitation to identify the natural frequencies and perform a modal analysis by measuring the plate response on a grid of points, (ii) harmonic excitation, increasing or decreasing by very small steps the excitation frequency in the spectral neighbourhood of the lowest natural frequencies to characterize nonlinear responses in presence of large-amplitude vibrations (step-sine excitation). The excitation has been provided by an electrodynamic exciter (shaker), model B&K 4810. A piezoelectric miniature force transducer



Fig. 2. Photograph of the experimental plate, connected to the shaker by the stinger and the load cell.

B&K 8203 of the weight of 3.2 g, placed on the plate at $x = a/4$ and $y = b/4$ and connected to the shaker with a stinger, measured the force transmitted. The plate response has been measured by using a very accurate laser Doppler vibrometer Polytec (sensor head OFV-505 and controller OFV-5000) in order to have non-contact measurement with no introduction of inertia. The time responses have been measured by using the Difa Scadas II front-end connected to a HP c3000 workstation and the software CADA-X of LMS for signal processing, data analysis and excitation control. The same front-end has been used to generate the excitation signal. The CADA-X closed-loop control has been used to keep constant the value of the excitation force for any excitation frequency, during the measurement of the nonlinear response.

Geometric imperfections of the plate have been measured by using a 3-D laser scanning system VI-910 Minolta. The contour plot indicating the deviation from the ideal flat surface is reported in Fig. 3. This figure shows that the actual shape of the plate is closer to a very shallow spherical shell; this is probably due to residual stresses of lamination in the steel foil and luser cut. Geometric imperfections are always present in actual plates, and their introduction in the present study has practical interest.

7.1. Linear results

The frequency response functions (FRFs) have been measured between 50 response points (7×7 points grid plus excitation point) and one single excitation point by using 8 averages and H_V technique. Excitation force and measured responses have been in z direction. The experimental modal analysis has been performed by using the software CADA-X 3.5b of LMS and burst-random excitation. The level of excitation was kept low in order to give small amplitude

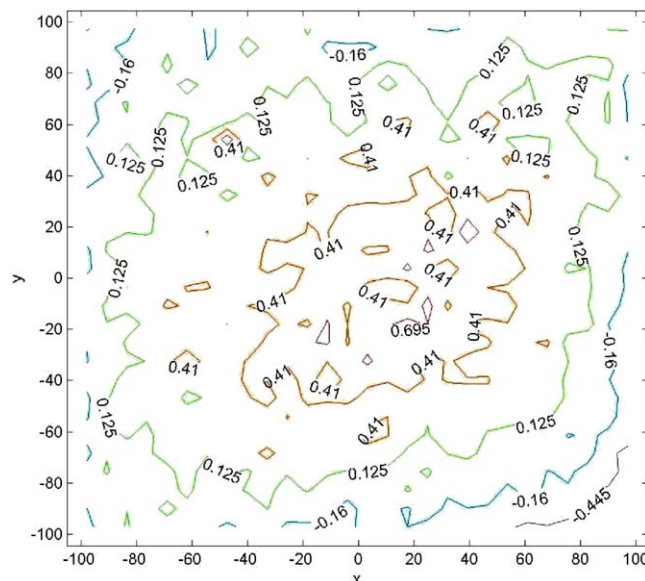


Fig. 3. Contour plot indicating measured geometric imperfections as deviation from the flat surface. Deviations are in millimeters.

Table 1
Natural frequencies of the experimental plate

Mode (m, n)	Experimental frequency (Hz)	Theoretical frequency without imperfection (Hz)
1, 1	38.7	32.7
1, 2	79.3	81.4
2, 1	90.4	82.1
2, 2	131.5	131
1, 3	162.1	163
3, 1	166.1	165

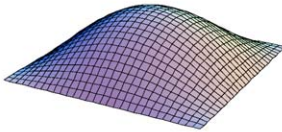
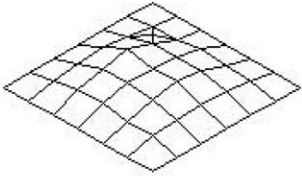
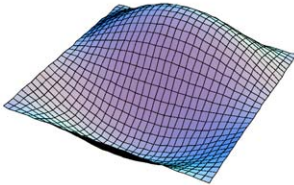
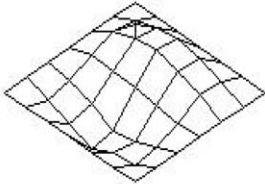
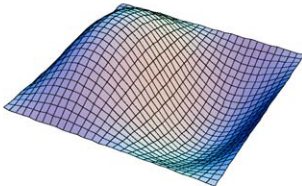
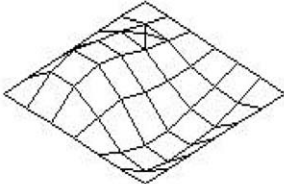
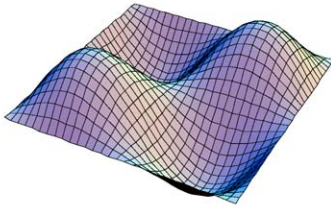
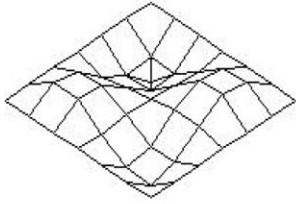
vibrations (approximating a linear system). Experimental and theoretical natural frequencies are given in Table 1; mode shapes are shown in Table 2. The agreement of natural frequencies is satisfactory, except for modes (1,1) and (2,1). It must be observed here that theoretical natural frequencies in Table 1 have been computed neglecting initial geometric imperfections, which play a significant role that will be shown. After introducing geometric imperfections, experimental and theoretical frequencies will become much closer, as it will be shown in the next sections. It can also be noticed that modes (1,2) and (2,1), that should have very close frequency because the plate is almost squared, have significant frequency separation. This suppresses the 1:1 internal resonance in the nonlinear analysis, and it is due to geometric imperfections.

7.2. Nonlinear results

Fig. 4 shows the measured oscillation (displacement, directly measured by using the Polytec laser Doppler vibrometer using the Polytec DD-200 displacement decoder (fringe counter for direct displacement measurement); measurement position at the center of the plate) around the fundamental frequency ($n = 1, m = 1$; experimental natural frequency 38.7 Hz) versus the excitation frequency for six different force levels: 0.001, 0.01, 0.02, 0.04, 0.08 and 0.1 N. The level of 0.001 N gives a very good evaluation of the natural (linear) frequency. The closed-loop control used in the experiments keeps the magnitude of the harmonic excitation force constant after filtering the signal from the load cell in order to use only the harmonic component with the given excitation frequency. The measured oscillation reported in Fig. 4 has been filtered in order to eliminate any frequency except the excitation frequency. Experiments have been performed increasing and decreasing the excitation frequency; the frequency step used in this case is 0.025 Hz, 32 periods have been measured with 64 points per period and 50 periods have been waited before data acquisition every time that the frequency is changed. The hysteresis between the two curves (up = increasing frequency; down = decreasing frequency) is clearly visible for the two larger excitation levels (0.08 and 0.1 N). Sudden increments (jumps) of the vibration amplitude are observed when increasing and decreasing the excitation frequency; these are characteristic of nonlinear behavior, in present case of hardening-type nonlinearity. The graph in Fig. 4 has been made non-dimensional by dividing the oscillation by the plate thickness h , and the excitation frequency by the natural circular frequency of mode (1,1).

The extremely interesting characteristics of Fig. 4 is that, for the excitation levels 0.01, 0.02 and 0.04 N, the response is of softening-type, turning to hardening-type for larger excitations, i.e. 0.08

Table 2
Natural mode shapes of the experimental plate

Mode	Theory	Experiment
1, 1		
1, 2		
2, 1		
2, 2		

and 0.1 N. Actually this peculiar nonlinear behavior is due to the initial geometric imperfection (curvature of the plate); a perfectly flat plate present only hardening-type nonlinearity. For excitation 0.1 N, when the vibration amplitude is equal to about 3.2 times the plate thickness, the

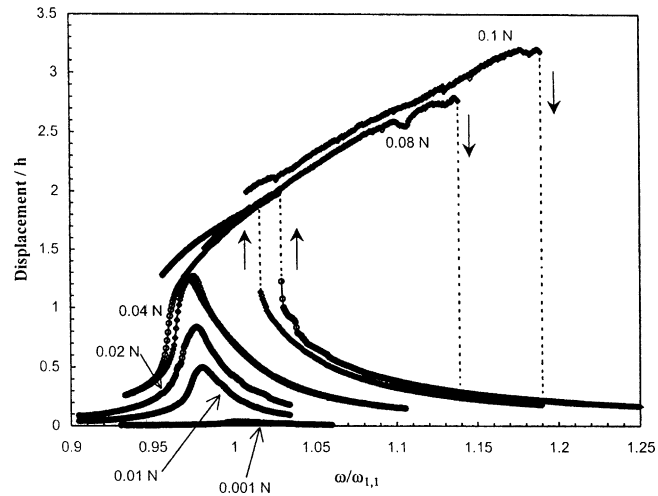


Fig. 4. Experimental non-dimensional oscillatory displacement (peak) versus non-dimensional excitation frequency for different excitations measured at the center of the plate; fundamental mode (1,1). \circ , experimental point; —, connecting line; \rightarrow , direction of movement along the line.

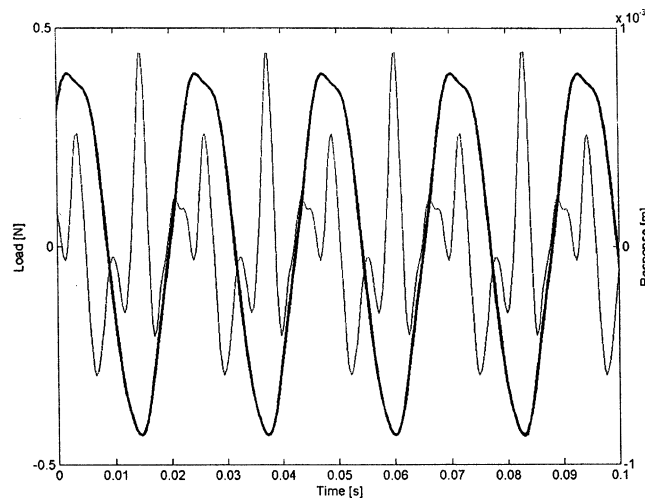


Fig. 5. Experimental results in time domain. —, force excitation; —, displacement response measured at the center of the plate. Mode (1,1), excitation frequency 43.97 Hz (increasing frequency, “up”) and excitation 0.08 N.

peak of the response appears for a frequency higher of about 19% with respect to the linear one (i.e. the one measured with force 0.001 N).

It must be observed that the force input around resonance was extremely distorted with respect to the imposed pure sinusoidal excitation. Fig. 5 shows the excitation and the measured response for excitation 0.08 N increasing the excitation frequency (“up”) at 43.97 Hz. While the response is largely filtered by the plate dynamics and it is not significantly distorted, the excitation is not

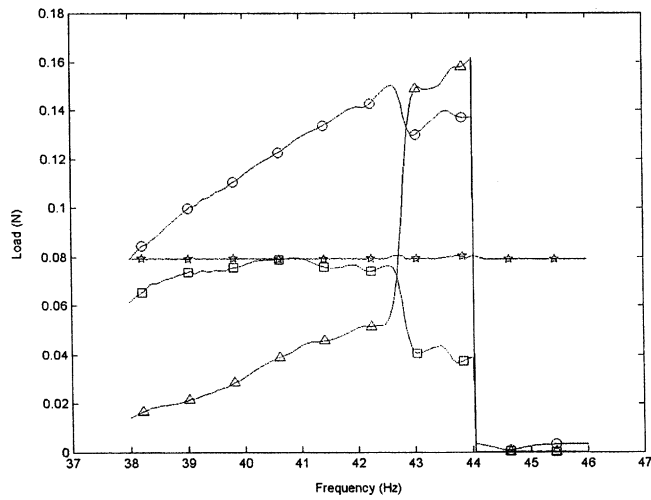


Fig. 6. Harmonic components of the excitation force. Mode (1,1); excitation 0.08 N up. ☆ = first harmonic; ○ = second harmonic; □ = third harmonic; △ = fourth harmonic.

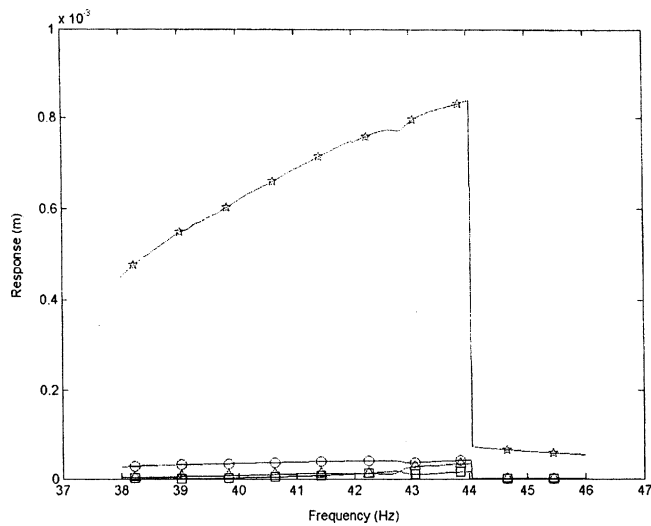


Fig. 7. Harmonic components of the displacement measured at the center of the plate. Mode (1,1); excitation 0.08 N up. ☆ = first harmonic; ○ = second harmonic; □ = third harmonic; △ = fourth harmonic.

sinusoidal at all. Fig. 6 shows the harmonic components in the excitation signal for this case in the frequency range investigated. In particular, the second and fourth harmonics of the excitation signal reaches amplitudes much larger than the first harmonic itself, which is the only one controlled. Fortunately in this case higher order harmonics do not have a significant effect on the plate dynamics, as shown by the harmonic components in the response signal shown in

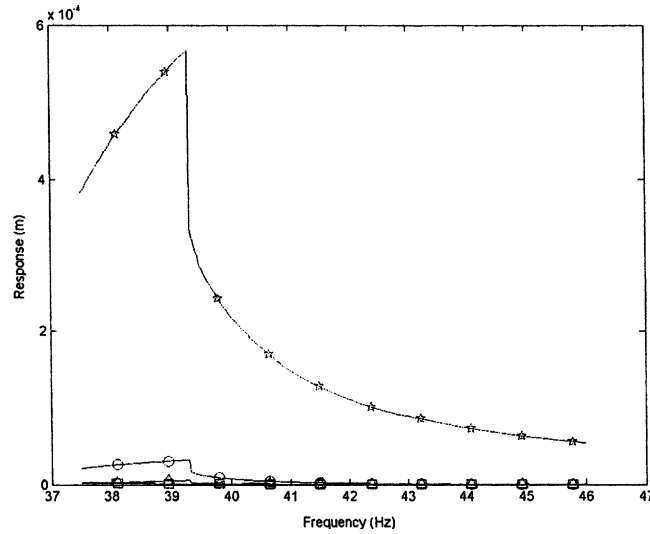


Fig. 8. Harmonic components of the displacement measured at the center of the plate. Mode (1,1); excitation 0.08 N down. ☆ = first harmonic; ○ = second harmonic; □ = third harmonic; △ = fourth harmonic.

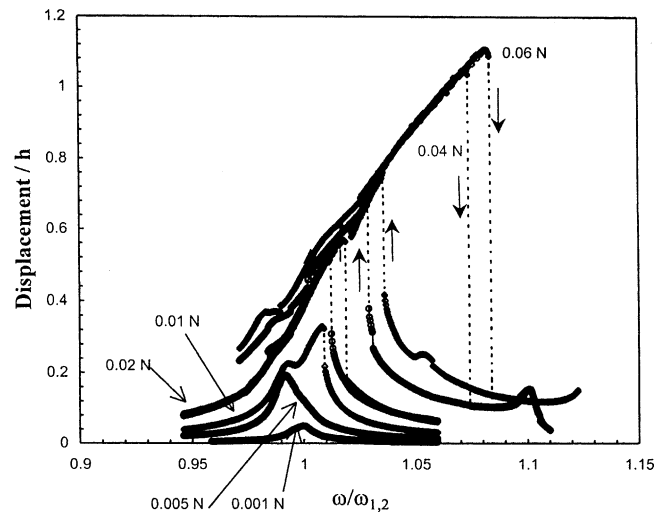


Fig. 9. Experimental non-dimensional oscillatory displacement (peak) versus non-dimensional excitation frequency for different excitation measured at $x = a/2$, $y = b/4$; mode (1, 2). ○, experimental point; - -, connecting line; →, direction of movement along the line.

Figs. 7 and 8 for excitation of 0.08 N “up” and “down”, respectively. As verified in a previous study for circular cylindrical shells [25], if higher harmonics are not directly exciting other modes, and it is not the case as shown by Figs. 7 and 8, their effect is small and they can be neglected in the theoretical model.

The nonlinear response of the plate around the second natural mode (1, 2) at 79.3 Hz is shown in Fig. 9. The response measurement has been effected at $x = a/2$, $y = b/4$, where the vibration amplitude of mode (1, 2) is maximum. Also in this case six different force levels have been used: 0.001, 0.005, 0.01, 0.02, 0.04 and 0.06 N. The level of 0.001 N gives a very good evaluation of the natural (linear) frequency. Initially a softening-type nonlinearity, due to geometric imperfections, is observed for small excitation levels; however, this effect is much smaller than in Fig. 4 for mode (1,1). Moreover, also internal resonances of type 2:1 with modes $w_{1,3}$ and $w_{3,1}$ are observed in secondary peaks (e.g. for the largest excitation, 0.06 N). For the three largest excitations, 0.02, 0.04 and 0.06 N, hardening-type nonlinearity is obtained with jumps. For vibration amplitude of about 1.1 times the plate thickness, the peak of the response appears for a frequency higher of about 8% with respect to the linear one, for the curve at 0.06 N.

8. Comparison of theoretical and experimental results

8.1. Mode (1,1)

A comparison of theoretical (22 dofs model with: $w_{1,1}$, $w_{1,3}$, $w_{3,1}$, $w_{3,3}$, $u_{1,0}$, $u_{1,2}$, $u_{1,4}$, $u_{3,0}$, $u_{3,2}$, $u_{3,4}$, $u_{5,0}$, $u_{5,2}$, $u_{5,4}$, $v_{0,1}$, $v_{2,1}$, $v_{4,1}$, $v_{0,3}$, $v_{2,3}$, $v_{4,3}$, $v_{0,5}$, $v_{2,5}$, $v_{4,5}$; in the choice of generalized coordinates symmetry considerations have been applied and geometric imperfections have been assumed to be symmetric) and experimental results is shown in Fig. 10(a) for two force levels (damping $\zeta_{1,1} = 0.0105$, forces 0.01 and 0.04 N) and in Fig. 10(b) for higher force level (damping

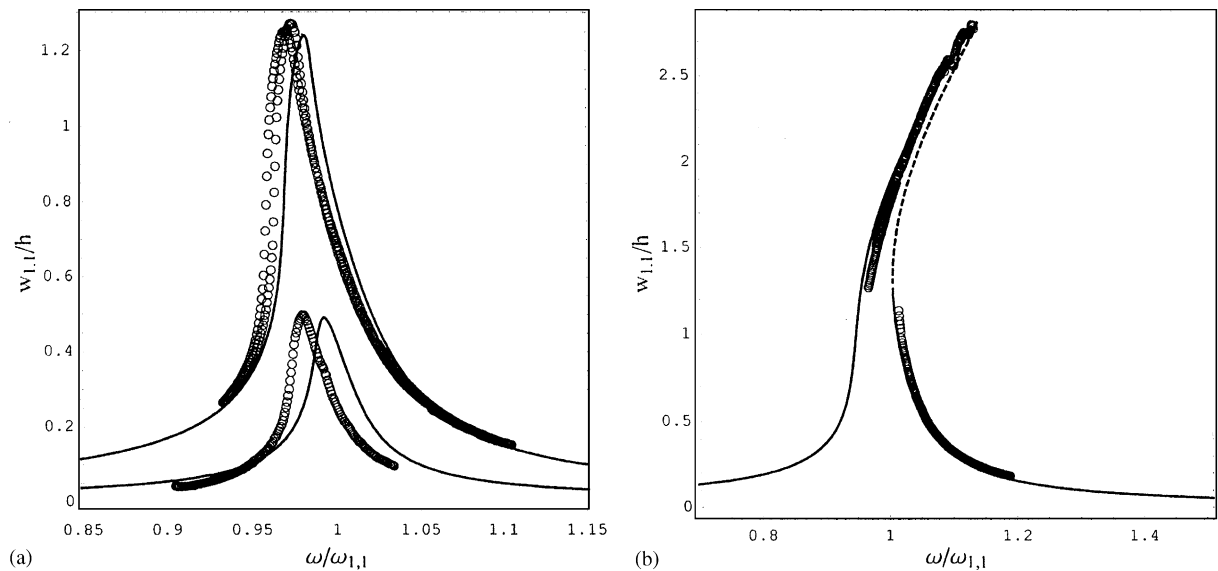


Fig. 10. Comparison of numerical and experimental results for the fundamental mode (1,1) at the center of the experimental plate; first harmonic only; $A_{1,1} = h$, $\zeta_{1,1} = 0.0105$; 22 dofs. \circ , experimental data; —, stable theoretical solutions; ---, unstable theoretical solutions. (a) $f = 0.01$ and 0.04 N; (b) $f = 0.08$ N.

$\zeta_{1,1} = 0.0105$, force 0.08 N); the same damping ratio is assumed for all the generalized coordinates. Comparison of numerical and experimental results is good for all the three cases; calculations have been obtained introducing the geometric imperfection $A_{1,1} = h$, having the form of mode (1,1), which is quite in agreement with the measured actual plate surface, as reported in Fig. 3 (measured imperfection at the center around 0.41 mm, which would give $A_{1,1} = 1.37h$ if the imperfection had the shape of mode (1,1)). The model with the introduced imperfection is perfectly capable to reproduce qualitatively and quantitatively the nonlinear behavior of the imperfect plate, with the initial softening-type behavior, turning to hardening-type for larger excitations and vibration amplitudes. It must be observed that in the figures the first harmonic of oscillation amplitude of the generalized coordinate $w_{1,1}$ is reported (therefore the mean value is eliminated), which is practically coincident with the first harmonic vibration amplitude of the plate at the center.

The six main generalized coordinates associated to the plate response given in Fig. 10(b) are reported in Fig. 11 for completeness. In particular, $w_{1,3}$ and $w_{3,1}$ give a significant quantitative contribution to the plate response.

The time responses of the generalized coordinates close to the response peak ($\omega = 1.135 \omega_{1,1}$) are given in Fig. 12 with their frequency spectra. In particular, the generalized coordinate $w_{1,1}$

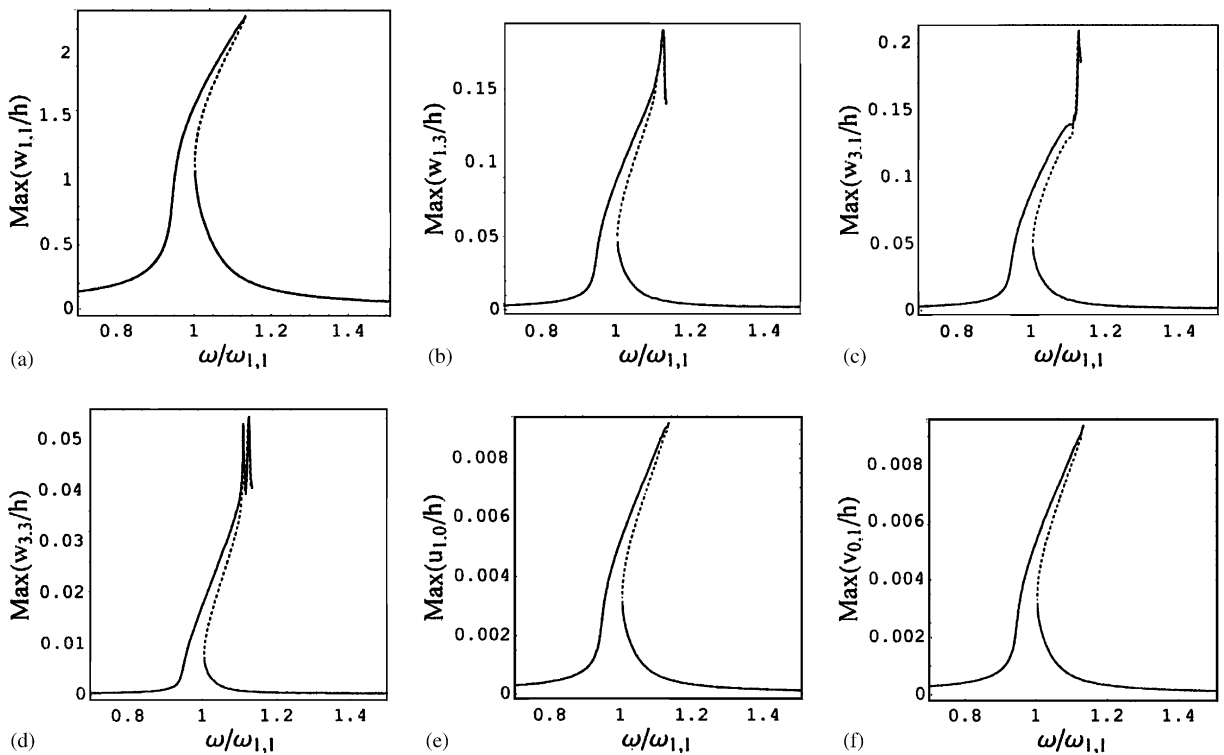


Fig. 11. Response of the plate; fundamental mode (1,1), $A_{1,1} = h$, $\tilde{f} = 0.08$ N and $\zeta_{1,1} = 0.0105$; 22 dofs. —, stable periodic response; - -, unstable periodic response. (a) Maximum of the generalized coordinate $w_{1,1}$; (b) maximum of the generalized coordinate $w_{1,3}$; (c) maximum of the generalized coordinate $w_{3,1}$; (d) maximum of the generalized coordinate $w_{3,3}$; (e) maximum of the generalized coordinate $u_{1,0}$; (f) maximum of the generalized coordinate $v_{0,1}$.

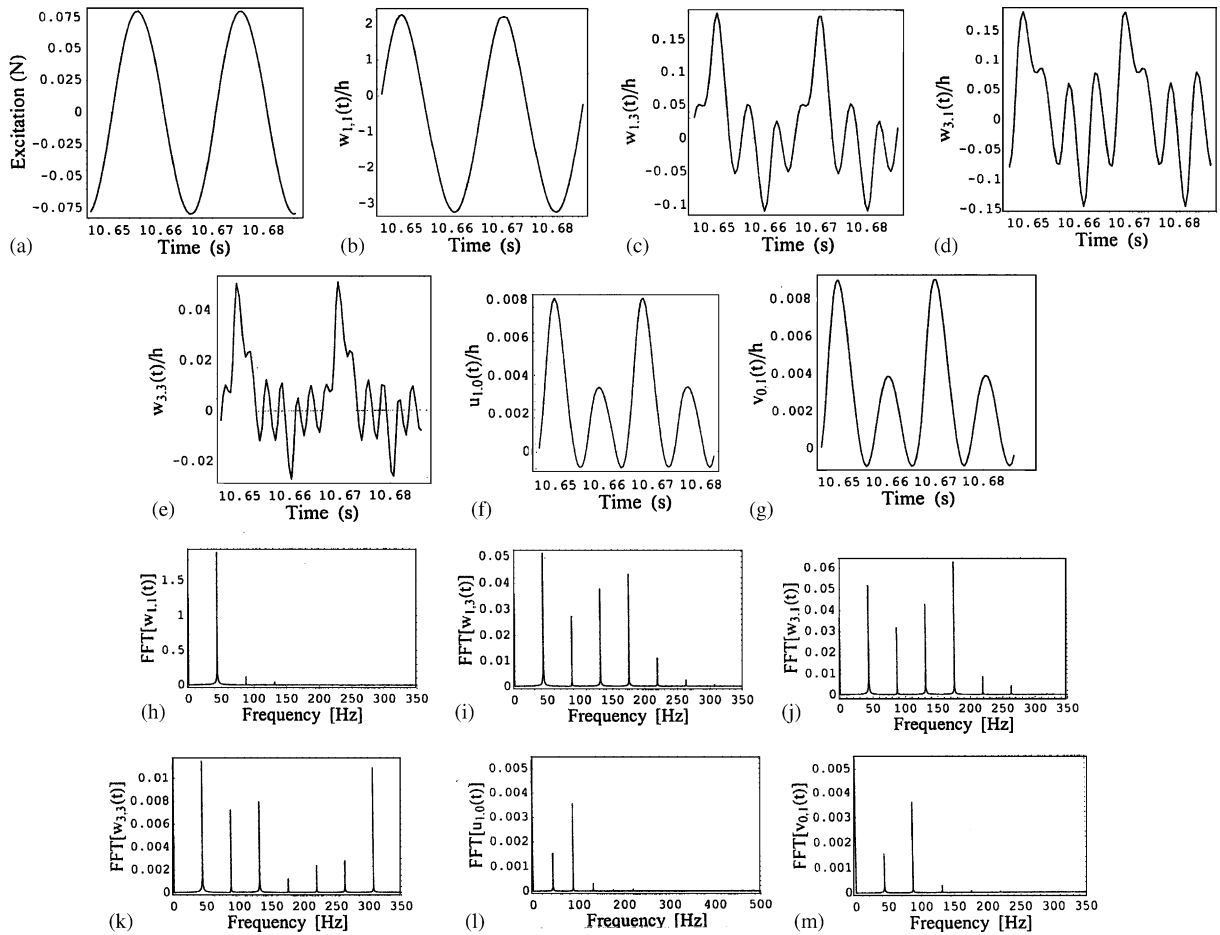


Fig. 12. Computed time response and frequency spectrum of the generalized coordinates; mode (1,1), $\omega = 1.135\omega_{1,1}$, $A_{1,1} = h$, $\hat{f} = 0.08$ N and $\zeta_{1,1} = 0.0105$; 22 dofs. (a) force excitation; (b) time response of $w_{1,1}$; (c) time response of $w_{1,3}$; (d) time response of $w_{3,1}$; (e) time response of $w_{3,3}$; (f) time response of $u_{1,0}$; (g) time response of $v_{0,1}$; (h) frequency spectrum of $w_{1,1}$; (i) frequency spectrum of $w_{1,3}$; (j) frequency spectrum of $w_{3,1}$; (k) frequency spectrum of $w_{3,3}$; (l) frequency spectrum of $u_{1,0}$; (m) frequency spectrum of $v_{0,1}$.

shows a large asymmetric displacement of the plate inwards and outwards the curvature created by the imperfection (a flat plate have symmetric displacement). This asymmetric displacement, resulting in a movement of the zero with respect to that of a sinusoidal oscillation, see Fig. 12(b), balance the imperfection around the resonance. In the frequency spectra, this zero harmonic is shown, as well as the second harmonic; these are due to quadratic nonlinearities in the equations of motion, introduced by geometric imperfections.

The convergence of the solution, versus the number of generalized coordinates retained in the expansion, is shown in Fig. 13. While the solution with 13 dofs is quite on the right-hand side, response computed with 22 and 38 dofs are very close, indicating convergence. The model with 13 dofs has: $w_{1,1}$, $u_{1,0}$, $u_{1,2}$, $u_{1,4}$, $u_{3,0}$, $u_{3,2}$, $u_{3,4}$, $v_{0,1}$, $v_{2,1}$, $v_{4,1}$, $v_{0,3}$, $v_{2,3}$, $v_{4,3}$. The model with 38 dofs has:

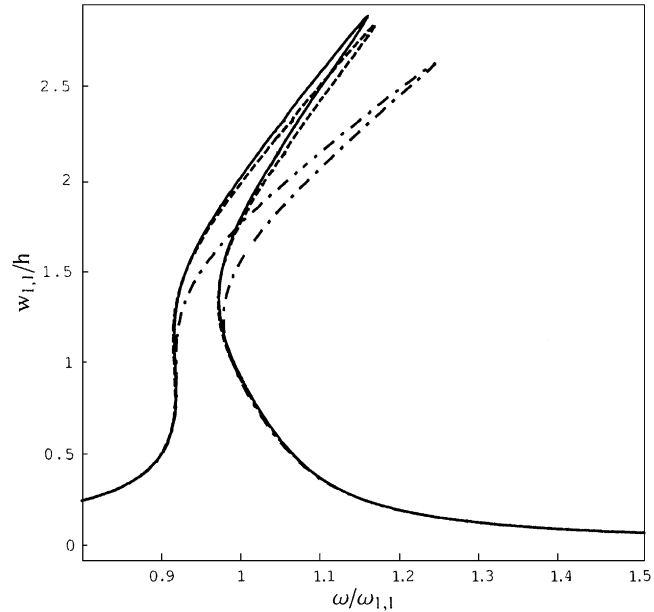


Fig. 13. Convergence of results; fundamental mode (1,1), $A_{1,1} = 1.25h$, $\tilde{f} = 0.105\text{ N}$ and $\zeta_{1,1} = 0.0105$. —, 38 dofs; --, 22 dofs; - · -, 13 dofs.

$w_{1,1}, w_{1,3}, w_{3,1}, w_{3,3}, w_{1,5}, w_{5,1}, u_{1,0}, u_{1,2}, u_{1,4}, u_{1,6}, u_{3,0}, u_{3,2}, u_{3,4}, u_{3,6}, u_{5,0}, u_{5,2}, u_{5,4}, u_{5,6}, u_{7,0}, u_{7,2}, u_{7,4}, u_{7,6}, v_{0,1}, v_{2,1}, v_{4,1}, v_{6,1}, v_{0,3}, v_{2,3}, v_{4,3}, v_{6,3}, v_{0,5}, v_{2,5}, v_{4,5}, v_{6,5}, v_{0,7}, v_{2,7}, v_{4,7}, v_{6,7}$.

The effect of the amplitude $A_{1,1}$ of geometric imperfection having the form of mode (1,1) on the nonlinear response is shown in Fig. 14. Smaller amplitudes of $A_{1,1}$ with respect to h do not allow the peculiar behavior found in the experiments. Fig. 14 shows that, after a while, all the curves for different initial imperfection become parallel each other. This asymptotic result is of significant relevance in applications.

The effect of $A_{1,1}$ on the natural frequency of the fundamental mode (1,1) is shown in Fig. 15. It is clearly shown that with $A_{1,1} = h$ the theoretical natural frequency raises from 32.7 Hz (see Table 1) to 38.5 Hz, becoming almost coincident to the experimental value of 38.7 Hz. Therefore the imperfection introduced perfectly describes the linear and nonlinear behavior of the experimental plate.

8.2. Mode (1,2)

A comparison of theoretical (36 dofs model with: $w_{1,2}, w_{1,1}, w_{1,3}, w_{3,1}, w_{3,3}, w_{1,4}, u_{1,1}, u_{1,3}, u_{1,5}, u_{3,1}, u_{3,3}, u_{3,5}, u_{1,0}, u_{1,2}, u_{1,4}, u_{3,0}, u_{3,2}, u_{3,4}, u_{5,0}, u_{5,2}, u_{5,4}, v_{0,2}, v_{2,2}, v_{4,2}, v_{0,4}, v_{2,4}, v_{4,4}, v_{0,1}, v_{2,1}, v_{4,1}, v_{0,3}, v_{2,3}, v_{4,3}, v_{0,5}, v_{2,5}, v_{4,5}$) and experimental results is shown in Fig. 16 (damping $\zeta_{1,2} = 0.0031$, force 0.04 N) and in Fig. 17 (damping $\zeta_{1,2} = 0.0035$, force 0.06 N); the same damping ratio is assumed for all the generalized coordinates except for $w_{1,3}$ and $w_{3,1}$ for which 0.01 is assumed in order to damp internal resonances. Comparison of numerical and experimental results is good for both cases; calculations have been obtained introducing the geometric imperfection $A_{1,1} = 1.25h$,

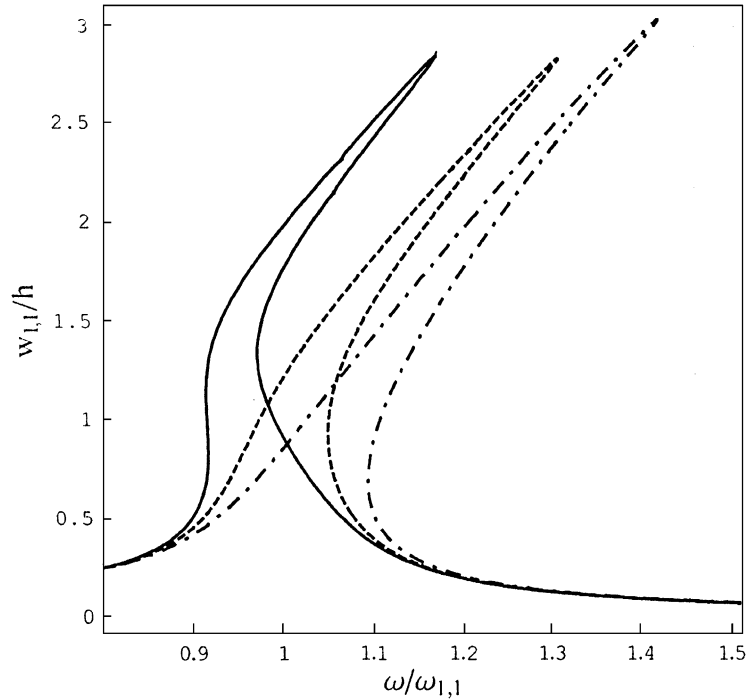


Fig. 14. Effect of geometric imperfection $A_{1,1}$ on the nonlinear response of the fundamental mode (1,1); $\tilde{f} = 0.105 N$ and $\zeta_{1,1} = 0.0105$. —, $A_{1,1} = 1.25h$; - -, $A_{1,1} = 0.75 h$; - · -, $A_{1,1} = 0$.

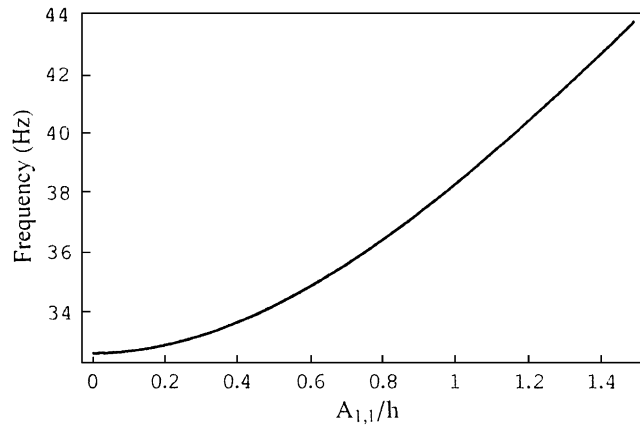


Fig. 15. Natural frequency of the fundamental mode (1,1) versus the geometric imperfection $A_{1,1}$.

having the form of mode (1,1), i.e. almost the same used to reproduce the experimental results for mode (1,1); here it was possible to keep the same imperfections to reproduce both modes (1,1) and (1,2) introducing more terms in the expansion of the imperfection, as it is actually in the experimental plate; natural frequency of mode (1,2) with the assumed imperfection is 88.6 Hz.

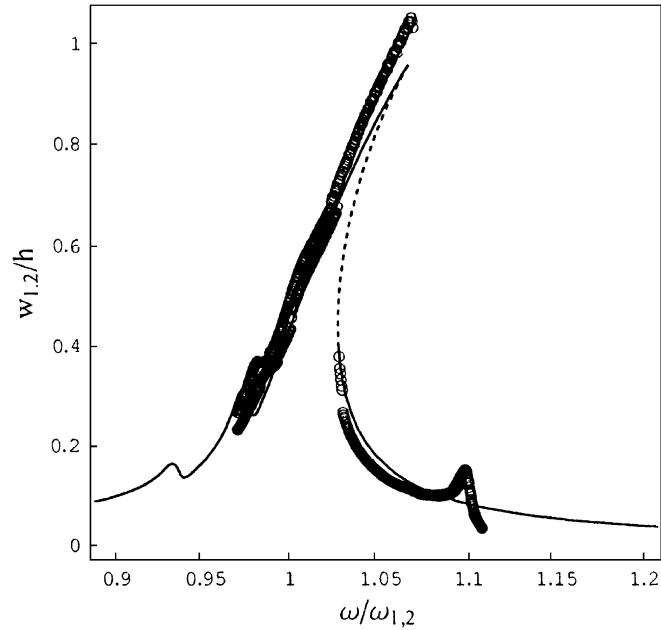


Fig. 16. Comparison of numerical and experimental results for mode (1,2) at $x = a/2$, $y = b/4$; first harmonic only; $A_{1,1} = 1.25 h$, $\varsigma_{1,2} = 0.0031$; $\hat{f} = 0.04 N$; 36 dofs. \circ , experimental data; —, stable theoretical solutions; ---, unstable theoretical solutions.

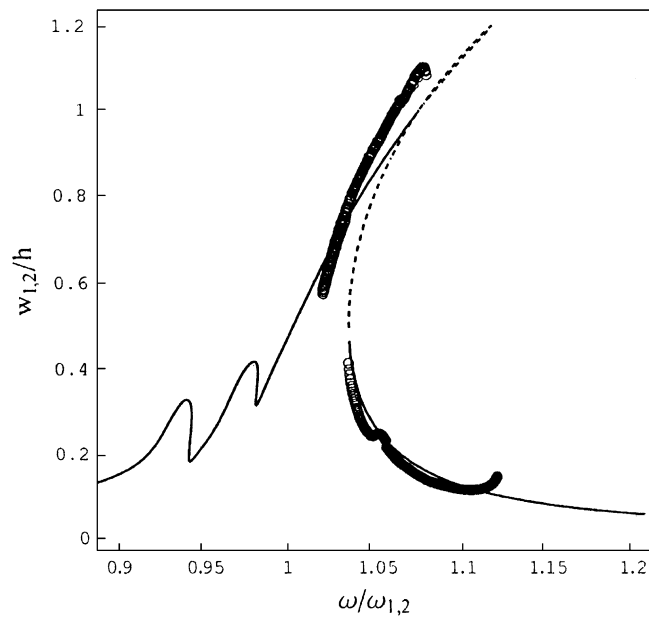


Fig. 17. Comparison of numerical and experimental results for mode (1,2) at $x = a/2$, $y = b/4$; first harmonic only; $A_{1,1} = 1.25 h$, $\varsigma_{1,2} = 0.0035$; $\hat{f} = 0.06 N$; 36 dofs. \circ , experimental data; —, stable theoretical solutions; ---, unstable theoretical solutions.

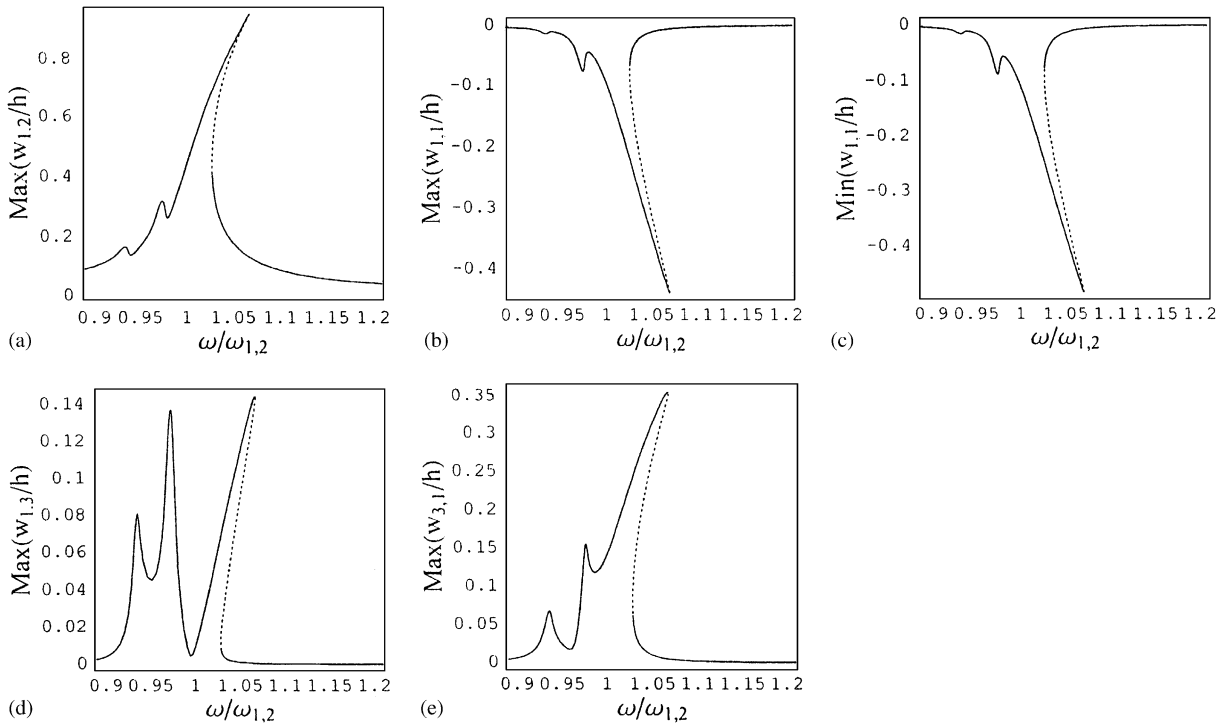


Fig. 18. Response of the plate; mode (1, 2), $A_{1,1} = 1.25 h$, $\tilde{f} = 0.004 \text{ N}$ and $\zeta_{1,2} = 0.0031$; 36 dofs. —, stable periodic response; - -, unstable periodic response. (a) maximum of the generalized coordinate $w_{1,2}$; (b) maximum of the generalized coordinate $w_{1,1}$; (c) minimum of the generalized coordinate $w_{1,1}$; (d) maximum of the generalized coordinate $w_{1,3}$; (e) maximum of the generalized coordinate $w_{3,1}$.

In Figs. 16 and 17 it is possible to observe secondary peaks associated to internal resonances of type 2:1 with modes (1,3) and (3,1). Small differences of frequencies of these peaks can be observed in the figures due to more complex geometric imperfection of the one introduced in the model, but they are present in both the model and the experiments. Moreover, the left-hand peak in Fig. 16 is almost perfectly predicted by the theory. Therefore, not only the nonlinear resonance has been described with good accuracy, but also internal resonances.

The four main generalized coordinates associated to the plate response given in Fig. 16 are reported in Fig. 18 for completeness. In particular, $w_{1,1}$, $w_{1,3}$ and $w_{3,1}$ give an extremely important quantitative contribution to the plate response $w_{1,2}$. The most important contribution $w_{1,1}$ is quasi-static, as shown by comparison of Figs. 18(b) and (c), where the maximum and the minimum displacements of the generalized coordinate $w_{1,1}$ are reported; this contribution reduces the amplitude of the geometric imperfection. In this case there is a more significant participation of generalized coordinates to the plate response than for fundamental mode (1, 1). Therefore, for mode (1,2) a correct expansion has to take into account more modes.

The time response of the most significant generalized coordinates and the corresponding spectra for excitation $\omega = 1.04\omega_{1,2}$ (damping $\zeta_{1,2} = 0.0031$, force 0.04 N , $A_{1,1} = 1.25 h$) are given in Fig. 19 and 20, respectively. The phase relationship and the frequency content of each

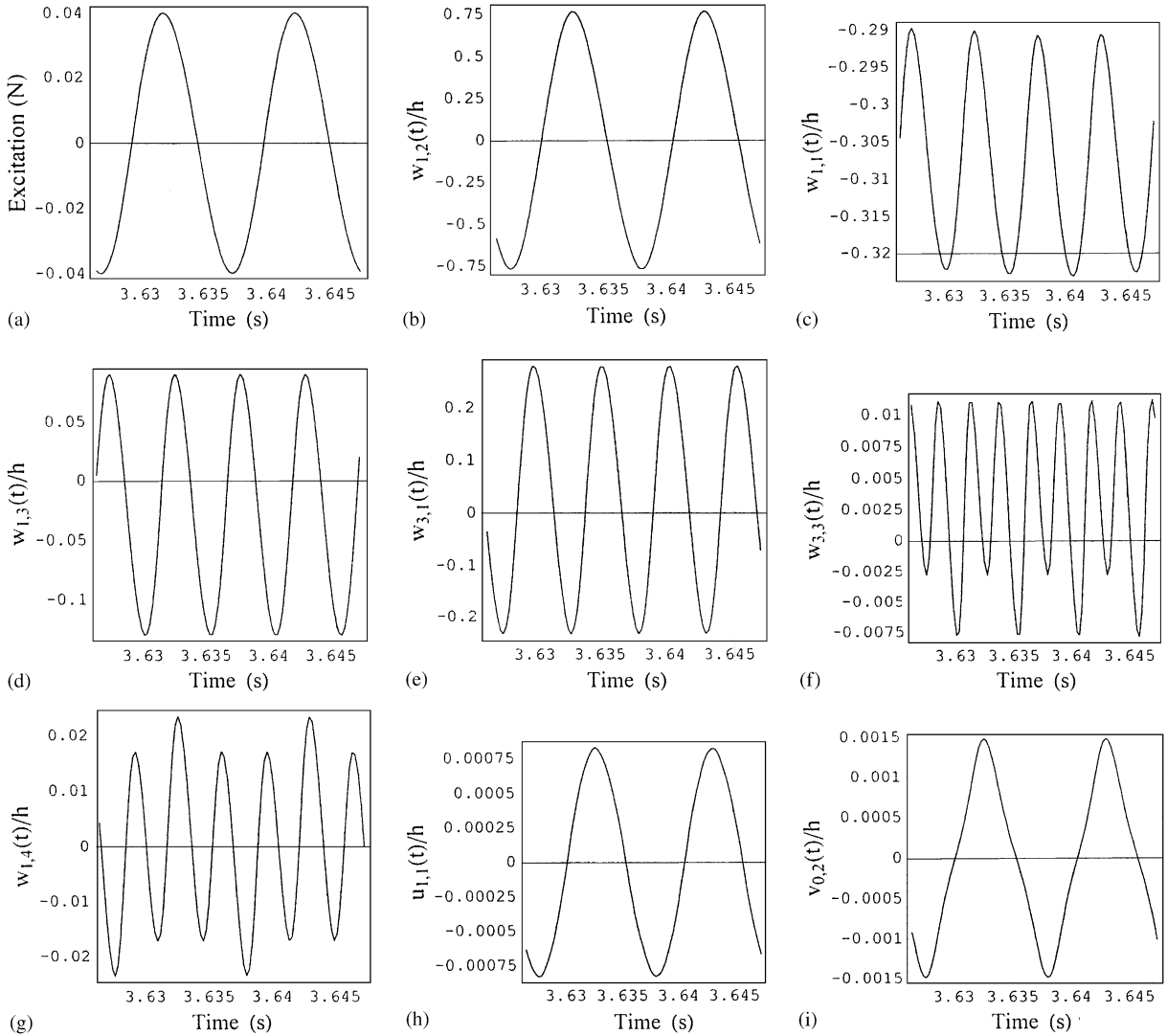


Fig. 19. Computed time response of the plate; mode (1, 2), $\omega = 1.04\omega_{1,2}$, $A_{1,1} = 1.25h$, $\tilde{f} = 0.004\text{ N}$ and $\zeta_{1,2} = 0.0031$; 36 dofs. (a) Force excitation; (b) Generalized coordinate $w_{1,2}$; (c) generalized coordinate $w_{1,1}$; (d) generalized coordinate $w_{1,3}$; (e) generalized coordinate $w_{3,1}$; (f) generalized coordinate $w_{3,3}$; (g) generalized coordinate $w_{1,4}$; (h) generalized coordinate $u_{1,1}$; (i) generalized coordinate $v_{0,2}$.

generalized coordinate is clearly shown. The quasi-static behavior of $w_{1,1}$ is confirmed; $w_{1,3}$ and $w_{3,1}$ participate with the second harmonic; $w_{3,3}$ contributes mainly with the fourth harmonic. It can be observed that the zero frequency component of $w_{1,1}$ and the second harmonic of $w_{1,3}$ and $w_{3,1}$ are related to quadratic nonlinearities.

Finally, the effect of the amplitude $A_{1,1}$ of geometric imperfection with the shape of mode (1,1) on the natural frequency of the fundamental mode (1,2) is shown in Fig. 21.

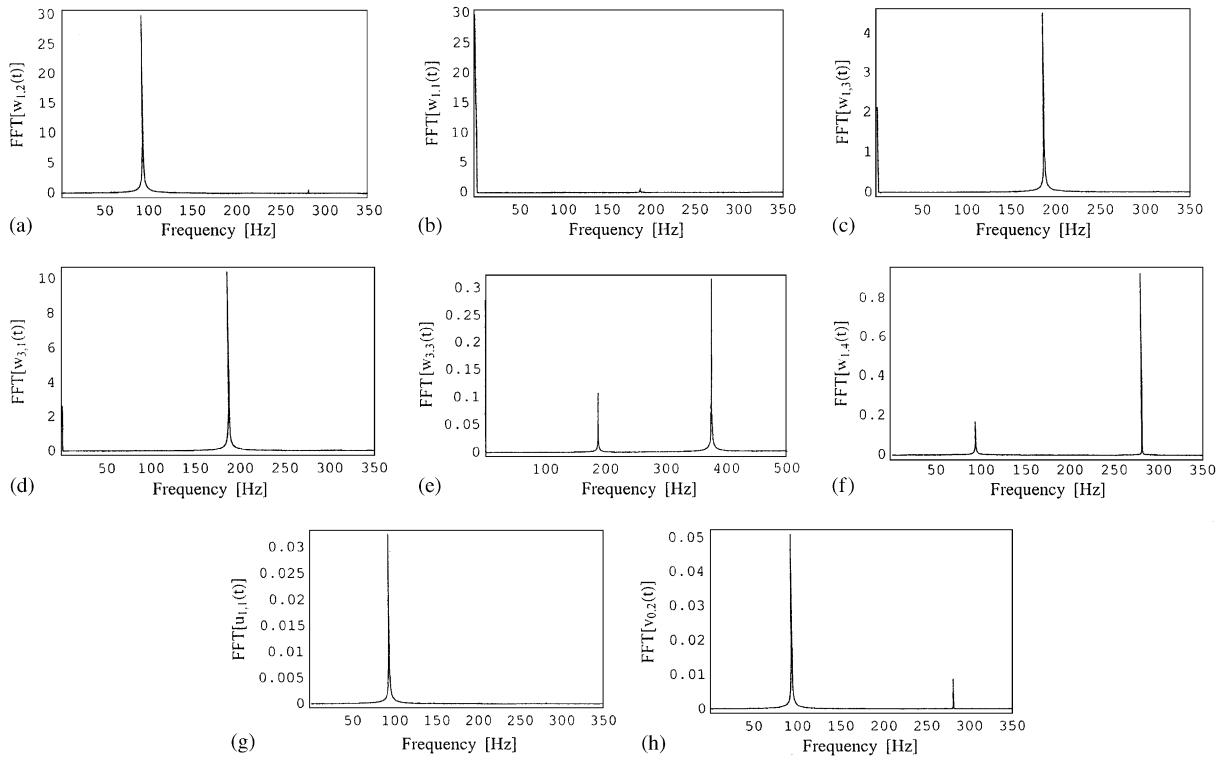


Fig. 20. Frequency spectrum of the response; mode (1, 2), $\omega = 1.04\omega_{1,2}$, $A_{1,1} = 1.25h$, $\tilde{f} = 0.004\text{ N}$ and $\zeta_{1,2} = 0.0031$; 36 dofs. (a) Generalized coordinate $w_{1,2}$; (b) generalized coordinate $w_{1,1}$; (c) generalized coordinate $w_{1,3}$; (d) generalized coordinate $w_{3,1}$; (e) generalized coordinate $w_{3,3}$; (f) generalized coordinate $w_{1,4}$; (g) generalized coordinate $u_{1,1}$; (h) generalized coordinate $v_{0,2}$.

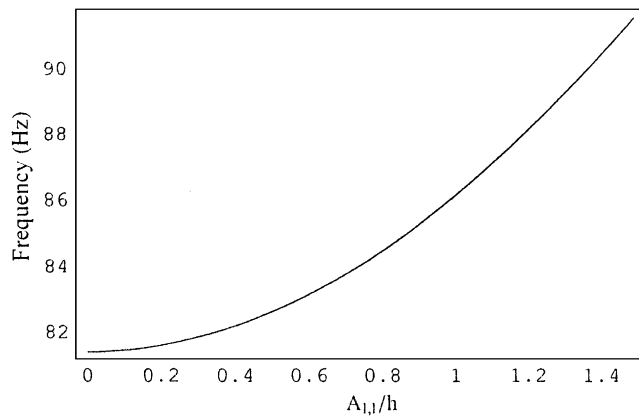


Fig. 21. Natural frequency of mode (1, 2) versus the geometric imperfection $A_{1,1}$.

It can be observed that in the 36 dofs model, in case of perfect plate, the following terms give zero contribution and therefore can be eliminated reducing the model to 20 dofs: $w_{1,1}$, $w_{1,3}$, $w_{3,1}$, $w_{3,3}$, $u_{1,1}$, $u_{1,3}$, $u_{1,5}$, $u_{3,1}$, $u_{3,3}$, $u_{3,5}$, $v_{0,2}$, $v_{2,2}$, $v_{4,2}$, $v_{0,4}$, $v_{2,4}$, $v_{4,4}$.

9. Conclusions

Experimental results on nonlinear vibrations of rectangular plates are extremely scarce in literature. With the present study new reliable results are given, which have been obtained with the most sophisticated instrumentation available at the moment. Moreover, these results have been reproduced with good accuracy by a model specifically developed in the present study to simulate the experimental boundary conditions. In particular, it has been shown that significant geometric imperfections can be present in actual plates and give an initial softening-type nonlinearity, which turns to hardening-type for larger amplitudes. Both the first and second modes have been experimentally and numerically investigated with success. This work partially fills the gap between existing studies on rectangular and circular plates [26–29], for which comparison of theoretical and experimental results has been already performed.

Acknowledgements

This work was partially supported by the FIRB 2001 and COFIN 2003 grants of the Italian Ministry for University and Research (MIUR). Ing. C. Augenti, A. Segalini, F. Vinci, and Dr. M. Pellegrini are thanked for helping the author in the experiments and some data processing. The support of company BPS (Ing. Broggi) at Pero (Milano, Italy), that provided the Polytec laser Doppler vibrometer, is acknowledged.

References

- [1] C-Y. Chia, *Nonlinear Analysis of Plates*, McGraw-Hill, New York, USA, 1980.
- [2] M. Sathyamoorthy, Nonlinear vibration analysis of plates: a review and survey of current developments, *Applied Mechanics Reviews* 40 (1987) 1553–1561.
- [3] C-Y. Chia, Geometrically nonlinear behavior of composite plates: a review, *Applied Mechanics Reviews* 41 (1988) 439–451.
- [4] M. Amabili, M.P. Païdoussis, Review of studies on geometrically nonlinear vibrations and dynamics of circular cylindrical shells and panels, with and without fluid-structure interaction, *Applied Mechanics Reviews* 56 (2003) 349–381.
- [5] H-N. Chu, G. Herrmann, Influence of large amplitude on free flexural vibrations of rectangular elastic plates, *Journal of Applied Mechanics* 23 (1956) 532–540.
- [6] M. Ganapathi, T.K. Varadan, B.S. Sarma, Nonlinear flexural vibrations of laminated orthotropic plates, *Computers and Structures* 39 (1991) 685–688.
- [7] S.R. Rao, A.H. Sheikh, M. Mukhopadhyay, Large-amplitude finite element flexural vibration of plates/stiffened plates, *Journal of the Acoustical Society of America* 93 (1993) 3250–3257.
- [8] A.Y.T. Leung, S.G. Mao, A symplectic Galerkin method for non-linear vibration of beams and plates, *Journal of Sound and Vibration* 183 (1995) 475–491.

- [9] Y. Shi, C. Mei, A finite element time domain modal formulation for large amplitude free vibrations of beams and plates, *Journal of Sound and Vibration* 193 (1996) 453–464.
- [10] D. Hui, Effects of geometric imperfections on large amplitude vibrations of rectangular plates with hysteresis damping, *Journal of Applied Mechanics* 51 (1984) 216–220.
- [11] K. Yasuda, T. Asano, Nonlinear forced oscillations of rectangular membrane with degenerated modes, *Bulletin of the JSME* 29 (1986) 3090–3095.
- [12] S.I. Chang, A.K. Bajaj, C.M. Krousgrill, Non-linear vibrations and chaos in harmonically excited rectangular plates with one-to-one internal resonance, *Nonlinear Dynamics* 4 (1993) 433–460.
- [13] W. Han, M. Petyt, Geometrically nonlinear vibration analysis of thin, rectangular plates using the hierarchical finite element method—I: the fundamental mode of isotropic plates, *Computers and Structures* 63 (1997) 295–308.
- [14] W. Han, M. Petyt, Geometrically nonlinear vibration analysis of thin, rectangular plates using the hierarchical finite element method—II: 1st mode of laminated plates and higher modes of isotropic and laminated plates, *Computers and Structures* 63 (1997) 309–318.
- [15] P. Ribeiro, M. Petyt, Geometrical non-linear, steady-state, forced, periodic vibration of plate, part I: model and convergence study, *Journal of Sound and Vibration* 226 (1999) 955–983.
- [16] P. Ribeiro, M. Petyt, Geometrical non-linear, steady-state, forced, periodic vibration of plate, part II: stability study and analysis of multi-modal response, *Journal of Sound and Vibration* 226 (1999) 985–1010.
- [17] P. Ribeiro, M. Petyt, Non-linear free vibration of isotropic plates with internal resonance, *International Journal of Non-Linear Mechanics* 35 (2000) 263–278.
- [18] P. Ribeiro, Periodic vibration of plates with large displacements, *Proceedings of the 42nd AIAA/ASME/ASCE/AHS/ASC Structures, Structural Dynamics, and Material Conference and Exhibit*, Seattle, WA, 2001, paper A01-25098.
- [19] M. El Kadiri, R. Benamar, Improvement of the semi-analytical method, based on Hamilton's principle and spectral analysis, for determination of the geometrically non-linear response of thin straight structures. Part III: steady state periodic forced response of rectangular plates, *Journal of Sound and Vibration* 264 (2003) 1–35.
- [20] M. Amabili, Nonlinear vibrations of rectangular plates with different boundary conditions: theory and experiments, *Computers and Structures* 82 (2004) 2587–2605.
- [21] Y.C. Fung, *Foundations of Solid Mechanics*, Prentice-Hall, Englewood Cliffs, NJ, 1965.
- [22] M. Amabili, Non-linear vibrations of doubly curved shallow shells, *International Journal of Non-Linear Mechanics* 40 (2005) 683–710.
- [23] S. Wolfram, *The Mathematica Book*, fourth ed., Cambridge University Press, Cambridge, UK, 1999.
- [24] E.J. Doedel, A.R. Champneys, T.F. Fairgrieve, Y.A. Kuznetsov, B. Sandstede, X. Wang, *AUTO 97: Continuation and Bifurcation Software for Ordinary Differential Equations (with HomCont)*, Concordia University, Montreal, Canada, 1998.
- [25] M. Amabili, Theory and experiments for large-amplitude vibrations of empty and fluid-filled circular cylindrical shells with imperfections, *Journal of Sound and Vibration* 262 (2003) 921–975.
- [26] N. Yamaki, K. Otomo, M. Chiba, Non-linear vibrations of a clamped circular plate with initial deflection and initial edge displacement, Part I: theory, *Journal of Sound and Vibration* 79 (1981) 23–42.
- [27] N. Yamaki, K. Otomo, M. Chiba, Non-linear vibrations of a clamped circular plate with initial deflection and initial edge displacement, Part II: experiment, *Journal of Sound and Vibration* 79 (1981) 43–59.
- [28] C. Touzé, O. Thomas, A. Chaigne, Asymmetric non-linear forced vibrations of free-edge circular plates. Part I: theory, *Journal of Sound and Vibration* 258 (2002) 649–676.
- [29] O. Thomas, C. Touzé, A. Chaigne, Asymmetric non-linear forced vibrations of free-edge circular plates. Part II: experiments, *Journal of Sound and Vibration* 265 (2003) 1075–1101.